Semiclassical study of nonsequential triple ionization of Ar in strong laser fields

Hui Jiang[1] and Feng He[1,2,*]

[1]*Key Laboratory for Laser Plasmas (Ministry of Education) and School of Physics and Astronomy, Collaborative Innovation Center for IFSA, Shanghai Jiao Tong University, Shanghai 200240, China*

[2]*CAS Center for Excellence in Ultra-intense Laser Science, Shanghai 201800, China*

(Received 8 June 2021; accepted 16 August 2021; published 27 August 2021)

We study nonsequential triple ionization of Ar in strong laser fields using a classical trajectory Monte Carlo simulation. By tracing electrons' trajectories, we reveal the mechanisms of triple ionization, including multiple recollision and sequential ionization. One electron tunnels out and rescatters with its parent ion, either kicking off two electrons together or kicking off one of them and exciting another one, which will be freed by the laser field. Besides the above-dominated channels, the cascade rescattering for triple ionization is explored, in which the first tunneling electron rescatters with the parent ion Ar^+ and kicks off the second electron and then the second electron gains energy in the laser field and rescatters with Ar^{2+}, kicking off the third electron or boosting it to excited states to be freed later. Such a cascade channel connects three electrons step by step, and Ar^{3+} may have larger ultimate momenta compared to the triple ionization mediated by only one rescattering. Our simulation shows it is possible to control the cascade channel and extract it through the ion momentum distribution.

DOI: 10.1103/PhysRevA.104.023113

I. INTRODUCTION

Atomic ionization is a central process in ultrafast physics. For single ionization, different ionization scenarios have been well understood, such as multiphoton ionization, tunneling ionization, and over-barrier ionization [1]. The ionization of atoms with one active electron can work as a benchmark to demonstrate fundamental physics, for example, the controversial debate about the tunneling time [2]. With the understanding of single ionization, double ionization (DI) in strong laser fields has been a hot topic since the 1990s [3]. The biggest difference from single ionization is that the electron correlation is overwhelmingly important for atoms at moderate laser intensities. The rescattering plays a central role in double ionization, in which one electron tunnels out and then is sent back to its parent ion by the laser field. During the collision, the rescattering electron may share its energy with another electron, directly kicking off the bound electron or boosting it to excited states, which will be freed by the laser field when the next wave crest comes. These two pictures are named nonsequential double ionization (NSDI) [4–8] and recollision-induced excitation with subsequent ionization (RESI) [9,10]. Some other mechanisms like "shake-off" [11] and "slingshot motion" [12] have been explored.

After the main mechanisms of DI were explored, researchers started to study triple ionization. The involvement of the third active electron makes the problem even more complex. Several experiments [13–18] showed that the atomic structure, the electron-electron correlation, and the laser wavelength play an important role in multiple ionization. These experiments also showed that the RESI mechanism may account for the triple-ionization channels [13,14]. Multiple ionization of Ar through multi-XUV-photon absorption has been studied [19]. Previously reported experiments mainly focused on the multiple-ionization rate as well as the ion momentum distribution.

Theoretically, it is hard to perform the *ab initio* simulations for triple ionization due to the large degrees of freedom. One possible way is to solve the time-dependent Schrödinger equation (TDSE) with reduced dimensionality. By confining the movement of three electrons along the laser polarization direction with a certain spin configuration, the time-dependent triple-ionization process with a high-frequency laser field was studied [20]. In Ref. [21], researchers used the time-dependent close-coupling method to study "a T-shape break-up pattern" in the triple photoionization of Li which has been predicted before [22,23]. Recently, a series of three-active-electron *ab initio* simulations [24–27] based on a certain geometry [28] studied the electron correlation under different spin configurations. Their intensity-dependent ionization yields are consistent with experiments [29] qualitatively. However, it is hard for a TDSE simulation to distinguish different ionization mechanisms such as RESI and sequential multiple ionization, and it will be very difficult to perform higher-dimensional TDSE simulations in the foreseeable future. Another widely used model is the classical-trajectory Monte Carlo simulation (CTMC). With this model, we can perform a three-dimensional simulation for three electrons, and the ionization mechanisms can be distinguished clearly. Recently, frustrated triple ionization in triatomic molecules was studied [30] with a classical model. Triple ionization for atoms was studied by purely classical CTMC [28,31–35]. In the model, the initial three active electrons are described by an ensemble having the atomic ground-state energy, and the dynamics are governed by the Newton equation for three

*fhe@sjtu.edu.cn

particles. Previous works [31,32,34,35] showed several channels for nonsequential triple ionization (NSTI) and explored the importance of rescattering. However, in the above study of the triple ionization, rescattering occurs only once, although multiple rescattering in double ionization was studied before [36]. One may expect the channels for triple ionization to be more complex since three active electrons are involved in the process. Therefore, a more systematic classification of ionization channels including multiple recollisions and sequential triple ionization (STI) needs to be developed.

In this paper, we perform semiclassical CTMC simulations to study the complex channels for triple ionization and focus on the cascade-rescattering-induced triple ionization. In our model, the single ionization is described by Ammosov-Delone-Krainov (ADK) theory [37], and the initial conditions of bound electrons are constructed using the Heisenberg-core potential [38,39] which was used successfully in previous works [40,41]. It should be noted that the Heisenberg-core potential has the potential to help us carry out a quantitative study on sequential multiple ionization classically [40]. Then, the evolution of the ensemble is governed by the Hamiltonian canonical equation including three electrons. By tracing the electrons' trajectories, we explore different triple-ionization channels, especially for cascade channels. The details of different channels, such as the ionization phase and corresponding nuclear momentum distribution, are analyzed. The rest of this paper is organized as follows. In Sec. II, we introduce the details of our simulation model. In Sec. III, we show the numerical results. The paper ends with a summary in Sec. IV.

II. NUMERICAL METHODS

We study the NSTI of Ar under a linearly polarized laser pulse. The laser field is expressed as $\mathbf{E}(t) = f(t)E_0 \sin\omega t\,\hat{\mathbf{x}}$, where $f(t)$ equals 1 for the first 10 cycles (unless otherwise specified) and reduces to zero linearly for the last three cycles, E_0 is the laser amplitude, and ω is the angular frequency. In the following calculations, we choose laser parameters for which the Keldysh parameter [42] is smaller than or around 1, and thus, the single ionization of Ar is described by ADK theory [37]. Hence, the tunneling rate can be expressed as $W_0(t) = 4(\frac{4I_{p1}}{E(t)})^{\frac{2}{\sqrt{2I_{p1}}}-1}\exp[\frac{-2(2I_{p1})^{\frac{3}{2}}}{3E(t)}]$, where $I_{p1} = 0.579$ is the single-ionization potential of Ar. The initial position of the tunneling electron (temporarily labeled e_3) is approximated by $\mathbf{x}_{3,0} = -\frac{I_{p1}}{|E(t)|}\hat{\mathbf{x}}$. The initial transverse momentum is approximated by Gaussian distribution with the width $\sqrt{\frac{|E(t)|}{2\sqrt{2I_{p1}}}}$, and the longitudinal momentum is assumed to be zero. The initial distribution of the two active bound electrons (e_1, e_2) is governed by the following Hamiltonian for Ar^+:

$$H_1 = \sum_{i=1}^{2}\left[\frac{1}{2}p_i^2 - \frac{3}{r_i} + V_H(r_i, p_i)\right] + \frac{1}{|\mathbf{r}_1 - \mathbf{r}_2|}, \quad (1)$$

where the Heisenberg-core potential [38] is written as

$$V_H(r_i, p_i) = \frac{(\xi_H\hbar)^2}{4\alpha r_i^2 m_e}\exp\left\{\alpha\left[1 - \left(\frac{r_i p_i}{\xi_H\hbar}\right)^4\right]\right\}. \quad (2)$$

Here, $\mathbf{r}_i$ is the position of the ith electron, and $\mathbf{p}_i$ is its canonical momentum. The parameter α in V_H indicates the strength of the Heisenberg constraint $r_i p_i \geqslant \xi_H\hbar$. Once α is given, we can choose the value of ξ_H to make the minimum of H_1 equal to the ground-state energy of Ar^+. The choice of α has little influence on the ground-state energy if α is not very small [43]. In our calculations, we set $\alpha = 4$, which was used in Ref. [43], and ξ_H is chosen to be 1.6352. The initial $\mathbf{r}_{i,0}$ and $\mathbf{p}_{i,0}$ of the two bound electrons can be obtained by minimizing H_1. To establish the two-electron classical ensemble, we rotate $\mathbf{r}_{i,0}$ and $\mathbf{p}_{i,0}$ with respect to the nucleus by a random angle [44] since H_1 is invariant under a rigid-body rotation. In our model of Ar^+, $r_1 = r_2 = 1.0939$, $p_1 = p_2 = 1.4949$, and the minimum of H_1 is -2.514, which equals the addition of the second ionization potential $I_{p2} = 1.016$ a.u. and the third ionization potential $I_{p3} = 1.498$ a.u. The Heisenberg-core potential was used successfully to study collisions with two-electron atoms [43] and the sequential multiple ionization [40], and its advantage is avoiding autoionization as well as constructing a good atomic structure classically comprising two active electrons.

We allocate the sampling number at different t according to the weight $W_0(t)$, where the tunneling instant t is uniformly distributed in the interval $[0, T]$ with the adjacent time separation $\Delta t = 0.37$ a.u. As far as we establish the ensemble for three electrons, we solve the canonical equations for the three-electron system in a strong laser field with the initial conditions we have introduced above,

$$\frac{d\mathbf{r}_i}{dt} = \frac{\partial H}{\partial \mathbf{p}_i}, \quad \frac{d\mathbf{p}_i}{dt} = -\frac{\partial H}{\partial \mathbf{r}_i}, \quad (3)$$

with the full Hamiltonian

$$H = \sum_{i=1}^{3}\left[\frac{1}{2}p_i^2 - \frac{3}{r_i} + V_H(r_i, p_i)\right] + \sum_{i,j=1;i<j}^{3}\frac{1}{|\mathbf{r}_i - \mathbf{r}_j|} + \sum_{i=1}^{3}\mathbf{r}_i \cdot \mathbf{E}(t). \quad (4)$$

In total, more than 10^9 trajectories are calculated in order to obtain converged results. The event is defined as triple ionization if all electrons finally have positive energies.

III. RESULTS

A. Different channels of triple ionization

In Fig. 1, we show the ionization yields for both DI and triple ionization (TI) under different laser intensities. Our simulation results show the common characters in rescattering-induced multiple ionization, and the results are comparable with those of previous works [24,27,31,45,46].

The CTMC calculations allow us to trace the trajectories of each electron, from which we are able to record the time-resolved velocity and energy. In Fig. 2 we present the typical time-dependent energy of three electrons for different channels. The laser intensity is $2.0 \times 10^{14}\,\mathrm{W/cm^2}$, and the wavelength is 800 nm. The triple-ionization rate is 0.205%. In our model, we define the ionization instant as the moment when the electron energy becomes positive. In order to classify different channels, we define the time interval between ionization and the corresponding rescattering as T_d. For

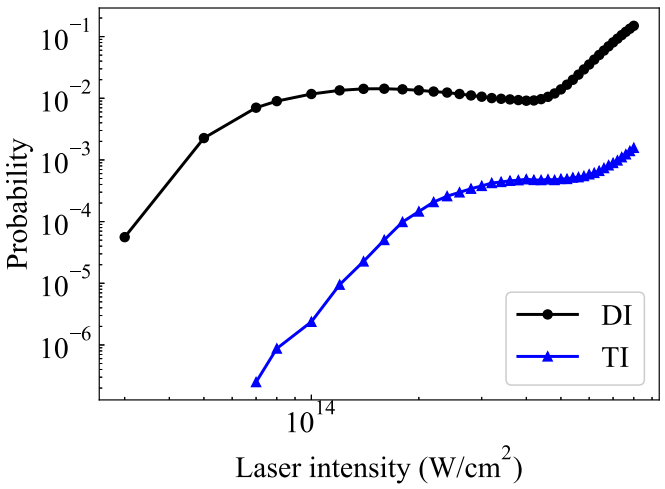

FIG. 1. The intensity-dependent ionization yields of Ar. The 800-nm laser field is linearly polarized with 5 cycles.

$T_d < 0.5T$, the rescattering and ionization happen in the same half optical cycle; that is, the electron is directly kicked off or escapes when the closest wave crest comes (the RESI-like mechanism).

For the laser parameters used in this paper, electron rescattering plays an important role. When the tunneling electron e_3 returns to its parent ion, it may kick off two electrons simultaneously if its rescattering energy is larger than $I_{p2} + I_{p3}$. However, if the rescattering energy of e_3 is smaller than $I_{p2} + I_{p3}$, it can kick off only one electron and leaves the third electron bounded. In this case, the ultimate triple ionization might require extra rescattering. Figures 2(a)–2(c) show the triple ionization that requires only one rescattering. As one can see in Fig. 2 (a), the two bound electrons emit together within the same half laser cycle after the first recollision. We define this channel as (1-3). In the titles above the panels in Fig. 2, a dash (-) represents recollision, while a tilde (∼) represents emission without direct recollision. The numbers in titles mean the number of freed electrons at each step of triple ionization. For example, (1-3) means before and after the rescattering, one and three electrons are freed, and the triple ionization is induced by rescattering. In Fig. 2(b), two electrons are freed after the first recollision, and the third electron is in an excited state. This excited electron is field ionized after an obvious delay larger than half a laser cycle. We define this channel as (1-2∼3). In Fig. 2(c), only e_2 is released after the rescattering within $0.5T$; the two electrons e_1 and e_3 are freed later by the remaining strong laser field. We define the channel as (1-1∼3). Channels (1-3) and (1-2∼3) were studied in Refs. [31,32,34,35] using a purely classical model. In addition to the above channels, some more complex channels for triple ionization are observed. Figures 2(d)–2(h) show the channels that require more than one recollision. In Fig. 2(d), e_2 escapes from Ar^+ after the first rescattering of e_3 at around $t = T$. Later, e_2 rescatters with Ar^{2+} and kicks off e_1 at around $t = 2T$. This is the cascade-rescattering triple ionization and is named (cas-1-2-3). A more detailed analysis of cascade rescattering will be given a little bit later. In Fig. 2(e) two recollisions happen; however, both recollisions are induced by the tunneling electron e_3. This channel is different from the cascade triple ionization we mentioned above, although quantum mechanically they do not resolve each other, and thus is defined as (noncas-1-2-3). In Fig. 2(f), the tunneling electron e_3 is captured by the nuclei during its rescattering; meanwhile, the two bound electrons e_1 and e_2 are freed within half a laser cycle. The remaining laser field drives e_2 back to e_3. This is also a cascade channel, and we name it (cas-1-2b-3). Here "2b" means that two freed electrons after the first recollision are the two bound electrons (e_1 and e_2). The scenarios in Fig. 2(g) and 2(h) are similar to that in Fig. 2(c), except that the bound electrons cannot be released without the second recollision. In Fig. 2(g), the two rescattering processes (around T and $2T$) are both caused by e_3, and we define the channel as (noncas-1-1-3). The scenario in Fig. 2(h) is as follows. During the first rescattering, e_3 and e_2 swap energy, and later on e_2 rescatters by kicking off e_1 and e_3 together; this process is named (cas-1-1-3). In Fig. 2(i), two bound electrons are released by the laser field without the rescattering of e_3, and we name it (1∼3). It should be noted that the time difference between triple ionization and the second recollision in (cas-1-2-3), (noncas-1-2-3), and(cas-1-2b-3) is smaller than half a laser cycle. However, the time difference could be larger than half a laser cycle, which means the electron is released by the laser with an obvious delay larger than $0.5T$, and we define these channels as (cas-1-2-3*), (noncas-1-2-3*), and(cas-1-2b-3*), respectively. These channels are not shown in Fig. 2.

More detailed studies show the channel (1∼3) actually include two scenarios. In the first case, three electrons are released one by one, and no recollision occurs at all. Thus, it is a purely sequential triple ionization. In the second case, the first electron gets freed from Ar, after which the second electron is freed sequentially. However, this second electron may come back and kick off the third electron. In the latter case, although the first electron is not correlated to the other two, the latter two are strongly correlated. We classify these two scenarios as (STI-1∼3) and (mix-1∼3), respectively. In Fig. 3, one can see that STI will dominate when the laser intensity is high. When the laser intensity is smaller than 2.0×10^{14} W/cm^2, STI has a very small probability, and rescattering-induced channels will dominate. In this work, we focus on the multiple-recollision channels.

Our CTMC calculations allow us to count the probabilities of different channels, as shown in Table I. The one-recollision triple ionization dominates. The channels listed in Table I take a total probability of about 95%. Some other channels, such as channels mediated by more than two recollisions, are not included in Table I.

B. Momentum distribution of ions

According to momentum conservation, one may calculate the ion momentum distribution once the electron momentum is obtained. In Fig. 4(a), we show the momentum distribution of Ar^{3+} along the laser polarization for different laser parameters, and the main characters of our results are consistent with previous experiments [13–16] and theoretical work [31,32,34,35]. According to the data in Table I, the three channels [(1-3), (1-2∼3), and (1-1∼3)] which require only one recollision have leading roles in the distribution of the total

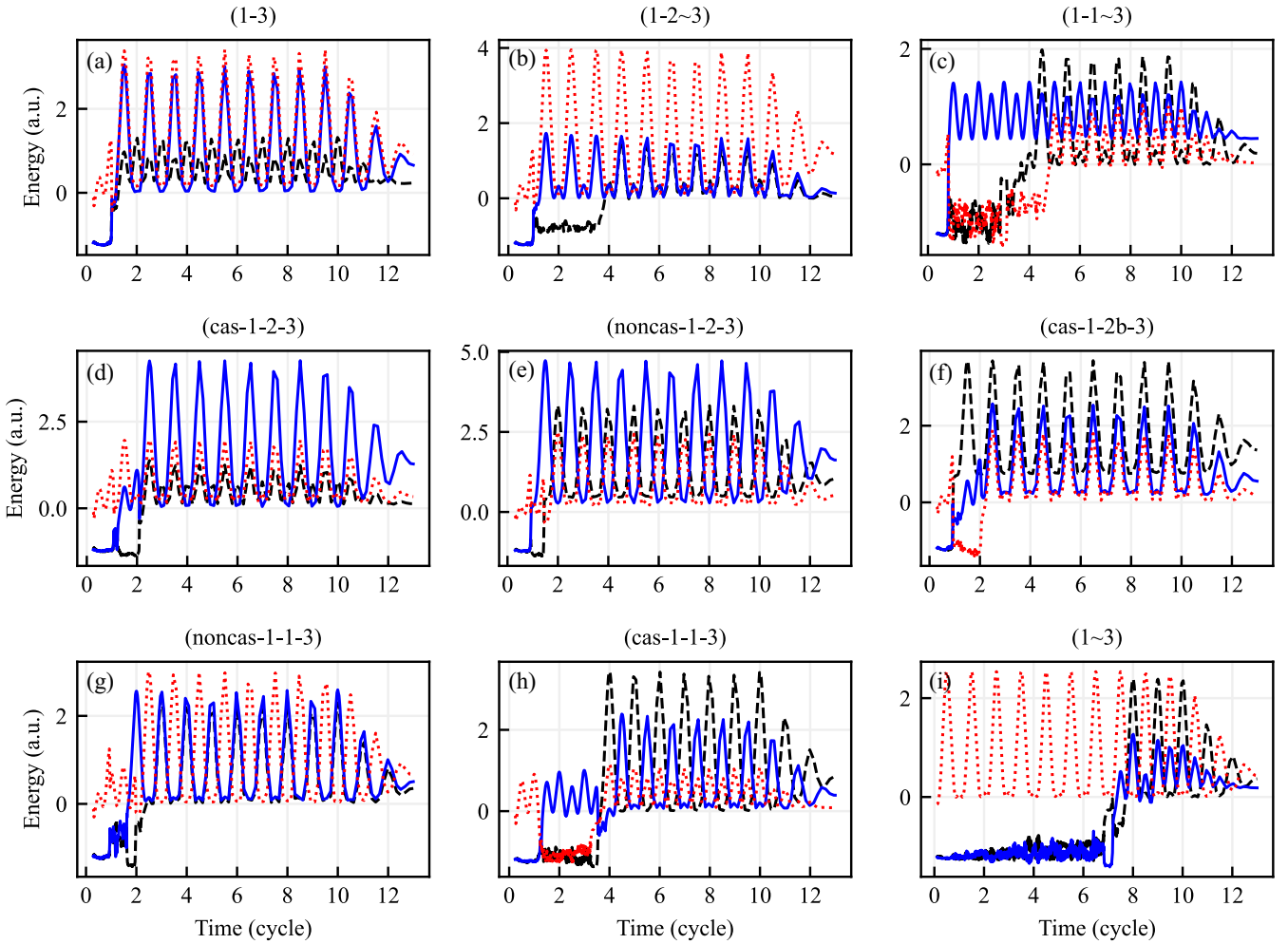

FIG. 2. Time evolutions of electron energies for the triple ionization of Ar. The dashed black, solid blue, and dotted red lines are for e_1, e_2, and e_3, respectively. The triple-ionization channels in different panels are marked at the top. The laser intensity is 2.0×10^{14} W/cm^2, the wavelength is 800 nm, and the pulse duration is 13 cycles.

ion momentum. Like in the extensive studies of ion momenta in double ionization, the double-hump structure shows the strong correlation between two electrons, while the filling of the valley between two humps indicates the contribution of sequential ionization or the RESI-like mechanism. The three lines in Figs. 4(b)–4(d) show the ion momentum distribution associated with channels (1-3), (1-2∼3), and (1-1∼3).

In Figs. 4(b)–4(d), channel (1-1∼3) has the same characters under different laser pulses. The ionization process in (1-1∼3) is strongly related to RESI mechanisms, leading to a total ion momentum close to zero. Also, one can see that the peak separation of channel (1-3) in Fig. 4(c) is wider than that in Fig. 4(b) and the momentum distribution of (1-3) in Fig. 4(b) is similar to that of (1-2∼3). The maximum kinetic energy carried by the recoil electron is approximated by $3.17U_p$ [47], with U_p being the ponderomotive energy. In Fig. 4(b), the maximum recoil energy equals 1.39 a.u., and it is smaller than $I_{p2} + I_{p3}$, so the tunneling electron can only pump the bound electrons to highly excited states, and the bound electrons are field ionized within $0.5T$ after the rescattering in channel (1-3). The three electrons emit within $0.5T$, and the ionization phase is around the laser wave crest. However, in Fig. 4(c) when the laser wavelength is 1200 nm, the maximum rescattering energy is up to 3.13 a.u. Therefore, the RESI mechanism in (1-3) is suppressed, and three electrons tend to emit simultaneously, leading to wider momentum distributions. When the rescattering energy is larger than $I_{p2} + I_{p3}$, the double peaks of (1-3) locate around $\pm 4\sqrt{U_p}$. The ion momentum distribution of (1-2∼3) is mainly determined by the first two released electrons since the last electron is released with a very small drift momentum. According to Figs. 4(b) and 4(d), the pulse length has little influence on the characters of different channels but modifies the proportions of different channels. For a shorter pulse, channel (1-1∼3) is suppressed, leading to more distinct double humps in the ion momentum distribution in Fig. 4(a). This result agrees with the experimental phenomena qualitatively [13]. One can see in Fig. 4(a) that it is hard to get high ion momentum around $\pm 6\sqrt{U_p}$ when the wavelength is 800 nm because the recoil energy of the tunneling electron is not large enough to release all electrons simultaneously. However, we can still get high ion momenta through cascade channels even when the wavelength is 800 nm, which will be discussed in the next section.

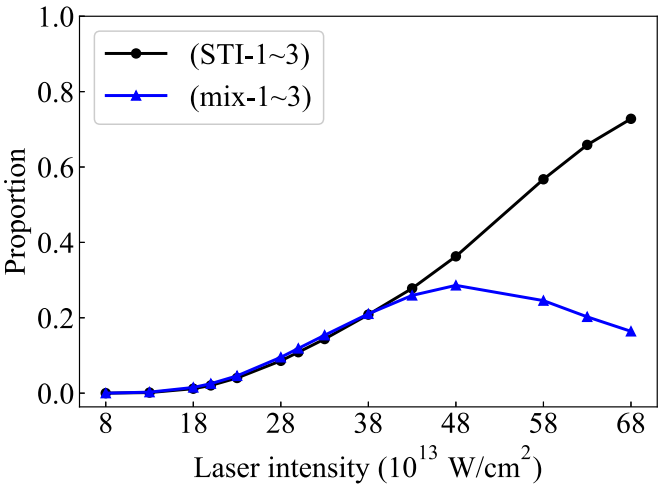

FIG. 3. Proportions of intensity-dependent sequential-involved triple-ionization channels for Ar. The 800-nm laser field is linearly polarized with 13 cycles. Here, (STI-1~3) means sequential triple ionization. (mix-1~3) means sequential double ionization followed by NSDI.

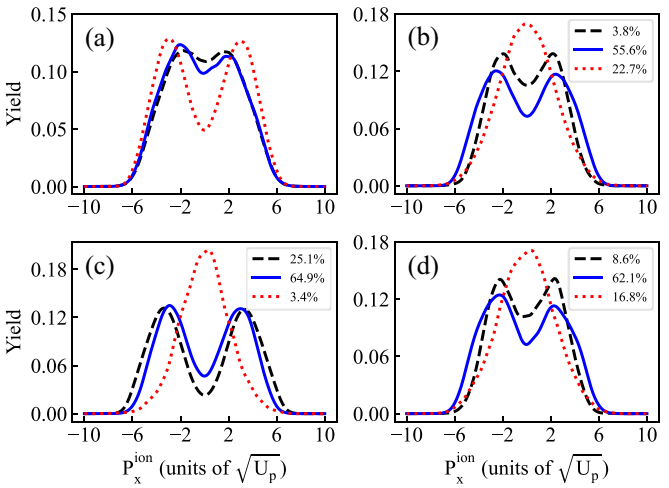

FIG. 4. The normalized final ion momentum distributions of Ar^{3+} along the polarization direction. The laser is linearly polarized along the $\hat{\mathbf{x}}$ direction. The laser intensity is 2.0×10^{14} W/cm^2. (a) The total ion momentum distribution for Ar^{3+} under different laser pulses. Dashed black line: 800 nm, 13 cycles; dotted red line: 1200 nm, 13 cycles; solid blue line: 800 nm, 7 cycles. (b)–(d) show the ion momentum distribution of three channels, where the dashed black line is for (1-3), the solid blue line is for (1-2~3), and the dotted red line is for (1-1~3). Labels in (b)–(d) show the proportions of the three channels. The laser parameters are 800 nm, 13 cycles in (b), 1200 nm, 13 cycles in (c), and 800 nm, 7 cycles in (d).

In general, when the laser intensity is very low and the maximum recoil energy is unable to release two bound electrons together, the (1-2~3) and (1-1~3) channels dominate the triple ionization. Because the momentum distribution of (1-1~3) exhibits a maximum at zero, the total ion momentum does not exhibit a clear double-peak structure. However, by increasing U_p, the recoil energy is larger, and electrons tend to emit directly after recollision, so the (1-1~3) channel is suppressed. In Fig. 5(a), we present the Ar^{3+} momentum distribution as a function of the wavelength at the fixed laser intensity 1.0×10^{14} W/cm^2. With the increase of the laser wavelength, the double-hump structure is more and more distinct. The proportions of the three main channels as a function of the laser wavelength are presented in Fig. 5(b).

C. Characters of cascade channels

In this section, we give a detailed analysis of the cascade channels named (cas-1-2-3) and (cas-1-2-3*). In Figs. 6(a)–6(c), we show the three channels of (cas-1-2-3*). In Fig. 6(a), e_1 jumps to an excited state after the second recollision and is released by the laser after half a laser cycle. In Fig. 6(b), e_1 gains enough energy and emits immediately just after the first recollision, but e_2 is frustrated into a bound state and released by the laser field after half a laser cycle. In Fig. 6(c), both e_1 and e_2 stay in excited states after the second rescattering and are released by the laser field after half a laser cycle. The scenario described by Fig. 6(c) has very few probabilities, and it is therefore not counted on in the later analysis.

TABLE I. Proportions of different channels in triple ionization. Parameters are the same as in Fig. 2.

Channel	Percentage	Channel	Percentage
(1-3)	3.8133	(cas-1-1-3)	0.5209
(1-2~3)	55.5797	(STI-1~3)	2.0464
(1-1~3)	22.7241	(mix-1~3)	2.4065
(cas-1-2-3)	1.0193	(cas-1-2-3*)	2.4016
(noncas-1-2-3)	0.6044	(noncas-1-2-3*)	1.4172
(cas-1-2b-3)	0.6579	(cas-1-2b-3*)	1.5793
(noncas-1-1-3)	0.5992		

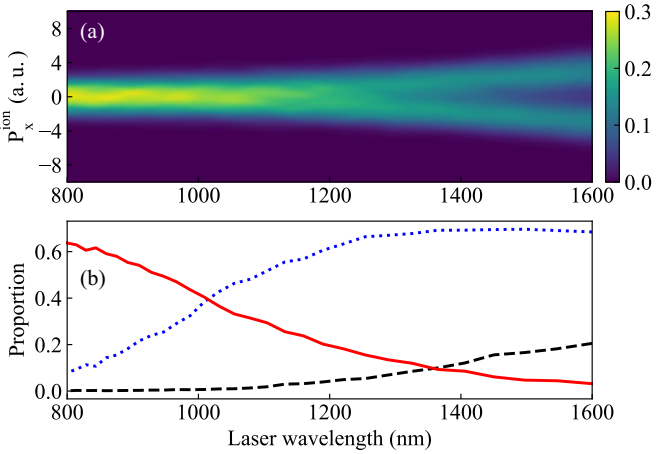

FIG. 5. (a) The ion momentum distribution of Ar^{3+}. (b) Proportions of different channels under different laser wavelengths; the dashed black line is for (1-3), the dotted blue line is for (1-2~3), and the solid red line is for (1-1~3) channels. The laser intensity is 1.0×10^{14} W/cm^2. The laser field is linearly polarized with 13 cycles.

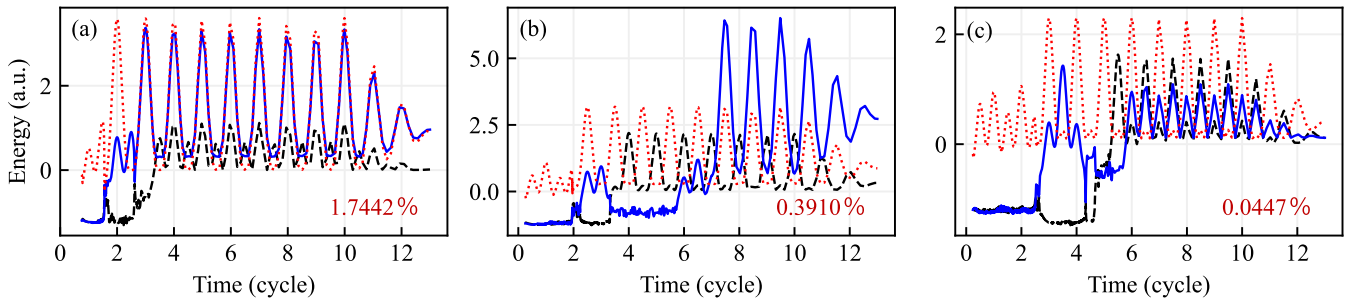

FIG. 6. Time evolution of electron energies for three types of (cas-1-2-3*). The dashed black, solid blue, and dotted red lines are for e_1, e_2, and e_3, respectively. Parameters of the laser pulse are the same as those in Fig. 2. The proportions of these channels are marked in the lower right.

To analyze the cascade channels conveniently, we define t_{r1} as the first rescattering instant of the tunneling electron e_3, t_{i1} as the ionization instant of e_2 caused by the first recollision, t_{r2} as the rescattering instant of e_2, and t_{i2} as the ionization instant of e_1. In Fig. 7, we show the phase distributions of ωt_{r1}, ωt_{i1}, ωt_{r2}, and ωt_{i2} in four columns. In Fig. 7, one can see that the tunneling electron returns to the nuclei right before the minimum of the laser field, after which e_2 emits within $0.5T$. In order to carry enough energy at the rescattering of e_2, the distribution of t_{i1} should be just after the maximum of the laser field, which is consistent with the simple-man model [48]. When e_2 returns to the nuclei, it carries the energy $K_r = \frac{E_0^2}{2\omega^2}[\cos(\omega t_{r2}) - \cos(\omega t_{i1})]^2$. Figures 7(b), 7(f) and 7(j) show that the distributions of the ionization phase of e_2 concentrate at $\pi/2$ and $3\pi/2$; hence, the main difference between these channels is the rescattering time of e_2. In Figs. 7(c), 7(g) and 7(k), one can see that the phase distribution of the second rescattering in (cas-1-2-3) is closer to zero and π than that in (cas-1-2-3*), so the recoil energy K_r in (cas-1-2-3) is larger than others, and e_1 can acquire enough energy to emit within $0.5T$. In Fig. 7(d), the maximum rescattering energy is about 1.39 a.u., which is a little smaller than I_{p3}; therefore, it is released around the maximum of the laser field within $0.5T$ when the closest wave crest comes. In Fig. 7(h), the distribution of the ionization phase is much broader than that in Fig. 7(d), and the excited electron e_1 emits after half a laser cycle. In Fig. 7(l), the distribution is similar to (cas-1-2-3) in Fig. 7(d), but one can see two additional small peaks at around 0.8π and 1.8π. Their positions are similar to the peak positions of t_{r2} in Fig. 7(k). For the scenario described in Fig. 6(b), e_1 emits within $0.5T$ after the recollision of e_2, but e_2 is frustrated into bound states, so the total energy that transfers from e_2 to e_1 is the addition of the energy of e_2 before t_{r2} and the bound energy of e_2 after recollision. When

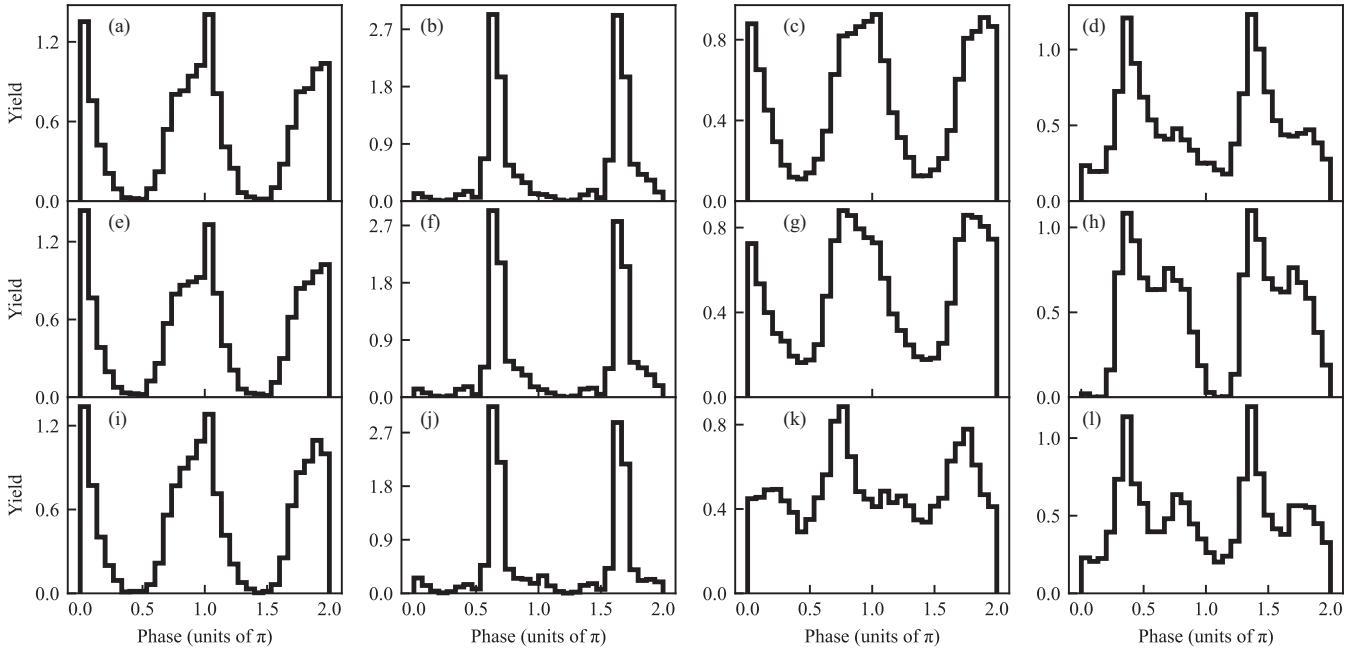

FIG. 7. Normalized phase distribution of different time points for different channels. Parameters of the laser pulse are the same as those in Fig. 2. Different rows represent different channels. The first row shows (cas-1-2-3), the second row shows the channel in Fig. 6(a), and the third row shows the channel in Fig. 6(b). The first column shows the phase distribution of t_{r1}; the other columns show the phase distributions of t_{i1}, t_{r2}, and t_{i2}, from left to right.

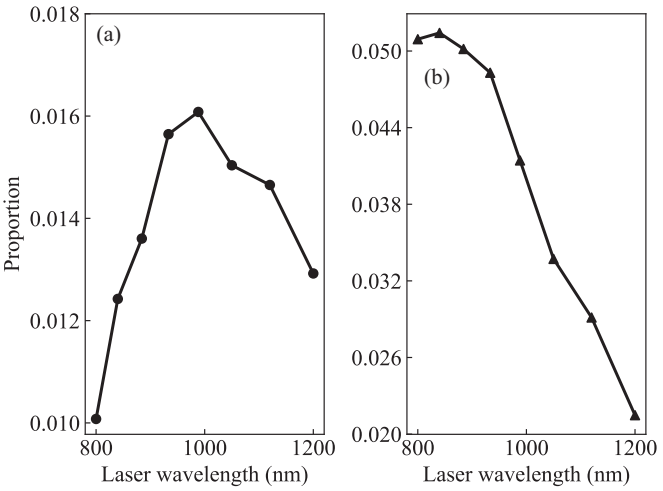

FIG. 8. The proportions of different cascade channels under different laser wavelengths. The laser intensity is $1.0 \times 10^{14}\,\mathrm{W/cm^2}$. The laser is linearly polarized with 13 cycles. (a) Proportions of channel (cas-1-2-3). (b) Proportions of channel (cas-1-2-3*).

the energy is larger than the bound energy of e_1, e_1 emits immediately. In such a case, t_{i2} is almost the same as t_{r2}.

Based on the above analysis, two factors are important to trigger cascade-rescattering triple ionization. First, the laser intensity should be proper to induce tunneling ionization, and it should not be too high to trigger the sequential ionization. Second, the ponderomotive energy should not be larger than $I_{p2} + I_{p3}$; otherwise, only one rescattering will induce the triple ionization. Also, the ponderomotive energy should not be too small since too small rescattering energy hardly kicks off or even excites the bound electron. In Fig. 8, we show the proportions of (cas-1-2-3) and (cas-1-2-3*) as a function of laser wavelengths. From Fig. 8(a), we can see that the proportion of (cas-1-2-3) has a maximum at a wavelength around 1000 nm and $3.17U_p = 1.09$, which is a bit larger than I_{p2}.

According to the simple-man model, the ultimate electron momentum in single ionization equals $\mathbf{p}_x = \mathbf{A}(t_0)$ [13,49] if the Coulomb potential is not included. Therefore, three electrons emitted at the same phase around zero or π would favor producing large ion momenta. However, for an 800-nm laser pulse as weak as $2.0 \times 10^{14}\,\mathrm{W/cm^2}$, the proportion of the (1-3) channel among all triple ionizations is about 3.8%, and only 0.26% events in the (1-3) channel have the character that three electrons emit simultaneously within $T/8$. So one-rescattering-induced direct triple ionization is almost impossible. However, with the help of cascade rescattering which has two recollisions, three electrons may emit at different periods but still have close phases. In Fig. 9(a), we show the distribution of the time difference between two recollision times (t_{r1} and t_{r2}). If the time difference is around nT (n is an integer less than the number of laser cycles), then the two recollisions happen at almost the same phase, and the electrons also emit with close phase. In Fig. 9(a), we choose cascade events that lie in the region $[nT - 0.1T, nT + 0.1T]$ (surrounded by red dotted lines), and the normalized ion momentum distribution is shown in Fig. 9(b). For the parameters we used, (cas-1-2-3) has a

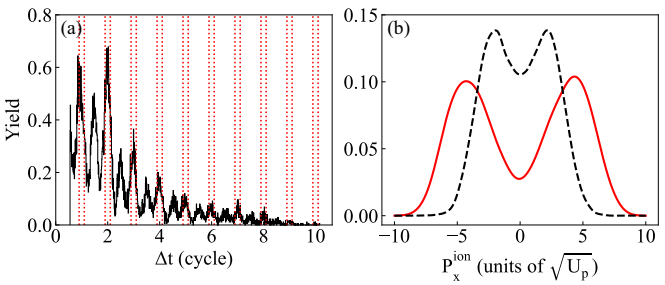

FIG. 9. (a) Distribution of the time difference between two recollision times (t_{r1} and t_{r2}) in channel (cas-1-2-3). The regions surrounded by dotted red lines lie in $[nT - 0.1T, nT + 0.1T]$. (b) The normalized ion momentum distribution of Ar^{3+} for different channels. Parameters of the laser pulse are the same as those in Fig. 2. The solid red line is for the selected cascade channel among (cas-1-2-3) in which $t_{r2} - t_{r1}$ lies in $[nT - 0.1T, nT + 0.1T]$. The dashed black line is for channel (1-3).

much larger probability than the direct triple ionization in which three electrons emit simultaneously within $T/8$. In Fig. 9(b), we can see that the ion momentum distribution of the selected cascade channel is much broader than that from channel (1-3) and it has a relatively large probability around $\pm 6\sqrt{U_p}$.

Figure 10 shows the correlated momentum spectra for the events surrounded by red dotted lines in Fig. 9(a). We can see in Fig. 10(a) that e_3 and e_2 tend to have the same final momentum because they emit almost at the same laser phase during different periods. Also, the recollision phase of the tunneling electron is around the minimum of the laser field, so the drift momentum of e_3 and e_2 is close to the maximum of the laser vector potential ($\pm 2\sqrt{U_p}$). After the recollision of e_2, e_1 emits with a time delay when the closest wave crest comes. Thus, e_1 tends to emit in the same direction as e_3 and e_2. However, the drift momentum of e_1 is relatively smaller than that of e_3 and e_2 because of the time delay. This is the reason why we cannot see a maximum value of the spectrum along the diagonal line in Fig. 10(b) compared with the spectrum in Fig. 10(a). According to the above analysis, we can understand why the ion momentum of the selected cascade channel can have a broader distribution.

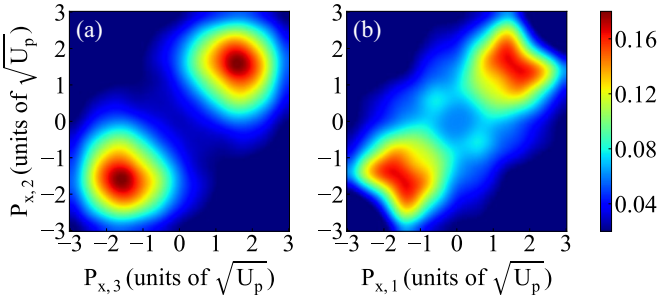

FIG. 10. The correlated momentum spectra between two electrons along the polarization direction for the selected cascade channel. (a) $e_2 - e_3$; (b) $e_2 - e_1$. The correlated momentum spectra show three electrons tend to emit in the same direction. e_3 is the tunneling electron, and e_1 and e_2 are the bound electrons in the initial ensemble.

IV. CONCLUSIONS

To summarize, we simulated the triple ionization of Ar in strong laser fields. By tracing the electrons' trajectories, we divided the events into various ionization channels. When the laser intensity is moderate and the rescattering energy is not large enough to kick off two bound electrons simultaneously, the cascade rescattering may contribute to triple ionization. For the cascade triple ionization in which the time difference between two recollisions is around nT, Ar^{3+} has distinct two humps in its momentum distribution. However, if the laser intensity is very strong, the sequential process dominates. If the laser wavelength is very long, channel (1-3) dominates; that is, the single ionized electron acquires enough energy and kicks off the two bound electrons together. In this case, the cascade rescattering has very small contributions. Looking forward, to extract the triple ionization contributed by the cascade rescattering, one may conceive a strategy of using an isolated attosecond pulse and a relatively weak infrared laser pulse, in which the attosecond pulse triggers single ionization and the infrared pulse steers the rescattering. By adjusting laser parameters, such as the time delays between the two pulses, the wavelength, and the intensity of the infrared pulse, the cascade rescattering may dominate the triple ionization.

ACKNOWLEDGMENTS

This work was supported by the Innovation Program of Shanghai Municipal Education Commission (Grant No. 2017-01-07-00-02-E00034), the National Key R&D Program of China (Grant No. 2018YFA0404802), and the National Natural Science Foundation of China (NSFC; Grants No. 11925405 and No. 91850203). Simulations were performed on the π supercomputer at Shanghai Jiao Tong University.

[1] M. Protopapas, C. H. Keitel, and P. L. Knight, Rep. Prog. Phys. **60**, 389 (1997).
[2] U. S. Sainadh, H. Xu, X. Wang, A. Atia-Tul-Noo, W. C. Wallace, N. Douguet, A. Bray, I. Ivanov, K. Bartschat, A. Kheifets, R. T. Sang, and I. V. Litvinyuk, Nature (London) **568**, 75 (2019).
[3] W. Becker, X. J. Liu, P. J. Ho, and J. H. Eberly, Rev. Mod. Phys. **84**, 1011 (2012).
[4] M. Lein, E. K. U. Gross, and V. Engel, Phys. Rev. Lett. **85**, 4707 (2000).
[5] P. J. Ho and J. H. Eberly, Phys. Rev. Lett. **95**, 193002 (2005).
[6] D. F. Ye, X. Liu, and J. Liu, Phys. Rev. Lett. **101**, 233003 (2008).
[7] J. Dubois, C. Chandre, and T. Uzer, Phys. Rev. Lett. **124**, 253203 (2020).
[8] A. Emmanouilidou, Phys. Rev. A **78**, 023411 (2008).
[9] B. Feuerstein, R. Moshammer, D. Fischer, A. Dorn, C. D. Schröter, J. Deipenwisch, J. R. Crespo Lopez-Urrutia, C. Höhr, P. Neumayer, J. Ullrich, H. Rottke, C. Trump, M. Wittmann, G. Korn, and W. Sandner, Phys. Rev. Lett. **87**, 043003 (2001).
[10] V. L. B. de Jesus, B. Feuerstein, K. Zrost, D. Fischer, A. Rudenko, F. Afaneh, C. D. Schröter, R. Moshammer, and J. Ullrich, J. Phys. B **37**, L161 (2004).
[11] D. N. Fittinghoff, P. R. Bolton, B. Chang, and K. C. Kulander, Phys. Rev. Lett. **69**, 2642 (1992).
[12] G. P. Katsoulis, A. Hadjipittas, B. Bergues, M. F. Kling, and A. Emmanouilidou, Phys. Rev. Lett. **121**, 263203 (2018).
[13] A. Rudenko, K. Zrost, B. Feuerstein, V. L. B. de Jesus, C. D. Schröter, R. Moshammer, and J. Ullrich, Phys. Rev. Lett. **93**, 253001 (2004).
[14] K. Zrost, A. Rudenko, Th. Ergler, B. Feuerstein, V. L. B. de Jesus, C. D. Schröter, R. Moshammer, and J. Ullrich, J. Phys. B **39**, S371 (2006).
[15] A. Rudenko, Th. Ergler, K. Zrost, B. Feuerstein, V. L. B. de Jesus, C. D. Schröter, R. Moshammer, and J. Ullrich, J. Phys. B **41**, 081006 (2008).
[16] O. Herrwerth, A. Rudenko, M. Kremer, V. L. B. de Jesus, B. Fischer, G. Gademann, K. Simeonidis, A. Achtelik, T. Ergler, B. Feuerstein, C. D. Schröter, R. Moshammer, and J. Ullrich, New J. Phys. **10**, 025007 (2008).
[17] N. Ekanayake, S. Luo, B. L. Wen, L. E. Howard, S. J. Wells, M. Videtto, C. Mancuso, T. Stanev, Z. Condon, S. LeMar, A. D. Camilo, R. Toth, W. B. Crosby, P. D. Grugan, M. F. Decamp, and B. C. Walker, Phys. Rev. A **86**, 043402 (2012).
[18] M. Schulz, R. Moshammer, W. Schmitt, H. Kollmus, R. Mann, S. Hagmann, R. E. Olson, and J. Ullrich, Phys. Rev. A **61**, 022703 (2000).
[19] A. Nayak, I. Orfanos, I. Makos, M. Dumergue, S. Kühn, E. Skantzakis, B. Bodi, K. Varju, C. Kalpouzos, H. I. B. Banks, A. Emmanouilidou, D. Charalambidis, and P. Tzallas, Phys. Rev. A **98**, 023426 (2018).
[20] C. Ruiz, L. Plaja, and L. Roso, Phys. Rev. Lett. **94**, 063002 (2005).
[21] J. Colgan, A. Emmanouilidou, and M. S. Pindzola, Phys. Rev. Lett. **110**, 063001 (2013).
[22] A. Emmanouilidou and J. M. Rost, J. Phys. B **39**, 4037 (2006).
[23] A. Emmanouilidou, P. Wang, and J. M. Rost, Phys. Rev. Lett. **100**, 063002 (2008).
[24] J. H. Thiede, B. Eckhardt, D. K. Efimov, J. S. Prauzner-Bechcicki, and J. Zakrzewski, Phys. Rev. A **98**, 031401(R) (2018).
[25] D. K. Efimov, J. S. Prauzner-Bechcicki, J. H. Thiede, B. Eckhardt, and J. Zakrzewski, Phys. Rev. A **100**, 063408 (2019).
[26] D. K. Efimov, J. S. Prauzner-Bechcicki, and J. Zakrzewski, Phys. Rev. A **101**, 063402 (2020).
[27] J. S. Prauzner-Bechcicki, D. K. Efimov, M. Mandrysz, and J. Zakrzewski, J. Phys. B **54**, 114001 (2021).
[28] K. Sacha and B. Eckhardt, Phys. Rev. A **64**, 053401 (2001).
[29] S. Palaniyappan, A. DiChiara, E. Chowdhury, A. Falkowski, G. Ongadi, E. L. Huskins, and B. C. Walker, Phys. Rev. Lett. **94**, 243003 (2005).
[30] M. B. Peters, V. P. Majety, and A. Emmanouilidou, Phys. Rev. A **103**, 043109 (2021).
[31] P. J. Ho and J. H. Eberly, Phys. Rev. Lett. **97**, 083001 (2006).
[32] P. J. Ho and J. H. Eberly, Opt. Express **15**, 1845 (2007).
[33] J. Guo and X.-S. Liu, Phys. Rev. A **78**, 013401 (2008).
[34] Y. Zhou, Q. Liao, and P. Lu, Opt. Express **18**, 16025 (2010).

[35] Q. Tang, C. Huang, Y. Zhou, and P. Lu, Opt. Express **21**, 21433 (2013).
[36] X. Ma, Y. Zhou, and P. Lu, Phys. Rev. A **93**, 013425 (2016).
[37] N. B. Delone and V. P. Krainov, J. Opt. Soc. Am. B **8**, 1207 (1991).
[38] C. L. Kirschbaum and L. Wilets, Phys. Rev. A **21**, 834 (1980).
[39] J. S. Cohen, Phys. Rev. A **51**, 266 (1995).
[40] Y. M. Zhou, C. Huang, Q. Liao, and P. X. Lu, Phys. Rev. Lett. **109**, 053004 (2012).
[41] S. Liu, D. Ye, and J. Liu, J. Phys. B **53**, 145005 (2020).
[42] L. V. Keldysh, Sov. Phys. JETP **20**, 1307 (1965).
[43] J. S. Cohen, Phys. Rev. A **54**, 573 (1996).
[44] J. S. Cohen, Phys. Rev. A **26**, 3008 (1982).
[45] M. Kübel, C. Burger, N. G. Kling, T. Pischke, L. Beaufore, I. Ben-Itzhak, G. G. Paulus, J. Ullrich, T. Pfeifer, R. Moshammer, M. F. Kling, and B. Bergues, Phys. Rev. A **93**, 053422 (2016).
[46] S. Augst, A. Talebpour, S. L. Chin, Y. Beaudoin, and M. Chaker, Phys. Rev. A **52**, R917 (1995).
[47] P. B. Corkum, Phys. Rev. Lett. **71**, 1994 (1993).
[48] T. F. Gallagher, Phys. Rev. Lett. **61**, 2304 (1988).
[49] B. Feuerstein, R. Moshammer, and J. Ullrich, J. Phys. B **33**, L823 (2000).